Effect of Hyperdiffusivity on Turbulent Dynamos with Helicity

Axel Brandenburg
NORDITA, Blegdamsvej 17, DK-2100 Copenhagen Ø, Denmark

Graeme R. Sarson
Department of Mathematics, University of Newcastle upon Tyne, NE1 7RU, United Kingdom
(Received 9 October 2001; published 18 January 2002)

In numerical studies of turbulence, hyperviscosity is often used as a tool to extend the inertial subrange and to reduce the dissipative subrange. By analogy, hyperdiffusivity (or hyperresistivity) is sometimes used in magnetohydrodynamics. The underlying assumption is that only the small scales are affected by this manipulation. In the present paper, possible side effects on the evolution of the large-scale magnetic field are investigated. It is found that for turbulent flows with helicity, hyperdiffusivity causes the dynamo-generated magnetic field to saturate at a higher level than normal diffusivity. This result is successfully interpreted in terms of magnetic helicity conservation, which also predicts that full saturation is reached only after a time comparable to the large-scale magnetic (hyper)diffusion time.

DOI: 10.1103/PhysRevLett.88.055003 PACS numbers: 52.65.Kj, 47.11.+j, 47.27.Ak, 47.65.+a

In theoretical studies of Navier-Stokes turbulence the ordinary viscosity operator, $\nu\nabla^2\boldsymbol{u}$, is sometimes replaced by $(-1)^{n-1}\nu_n\nabla^{2n}\boldsymbol{u}$, where ν_n is a hyperviscosity of order n. The use of hyperviscosity has the advantage of making the transition from the inertial subrange to the viscous subrange shorter [1]. At the same time, however, it has the notorious disadvantage of tempering possibly major parts of the inertial subrange. An example is the so-called bottleneck effect that leads to significantly shallower power spectra at high wave numbers near and before the viscous subrange [2]. When early simulations using the piecewise parabolic method showed such bottleneck effect [3], it was unclear whether this effect was real or just a consequence of hyperviscosity. In the context of magnetohydrodynamics, recent comparisons between direct and hyperviscous simulations point now to the latter possibility [4].

The use of hyperviscosity is indeed quite popular in studies of hydromagnetic turbulence where, in addition to viscosity, the ordinary magnetic diffusivity is replaced by hyperdiffusivity [4–7]. A strong artificial bottleneck effect occurs when hyperdiffusivity is used [4]. This is particularly clear in two dimensions at very high resolution [5], although a weak bottleneck effect occurs even without any hyperdiffusive effects [6]. The use of hyperviscosity and hyperdiffusivity has also led to significant controversy [8] in models of the Earth's dynamo [9]. At the center of the controversy is the effect of hyperviscosity on the asymptotic behavior at small Ekman number (low viscosity). This can also affect conclusions regarding the relative importance of the Lorentz force, and the relevance of Taylor's constraint, both matters of great importance for geodynamo theory. There are also examples where the use of hyperdiffusivity has moved dynamos from an α^2 regime toward an $\alpha\Omega$ regime [10].

Generally speaking, hyperviscosity and hyperdiffusivity can lead to rather ill-understood behavior that tends to diminish its potential advantages. It is therefore important to clarify exactly how hydromagnetic dynamos are affected by this approach. Here we concentrate on the effects of (magnetic) hyperdiffusivity. This is done in the context of MHD turbulence; future work will look at this effect on geodynamo models.

In the present paper we show that, if the fluid motions are helical, hyperdiffusivity can lead to artificially enhanced saturation amplitudes of the nonlinear dynamo. It is at first glance somewhat counterintuitive that the properties of the *large-scale* field should depend on the details of the diffusion operator, which is supposed to affect only the small scales. In recent years, however, there has been mounting evidence that large-scale dynamos, which usually involve helicity, do depend on the microscopic diffusion [11]. This property is related to magnetic helicity conservation, which permits magnetic helicity to change only on a resistive time scale; see Ref. [12], hereafter referred to as B2001. These processes can be seriously affected by the use of hyperdiffusivity. Obtaining a detailed understanding of the associated artifacts is crucial before hyperdiffusivity can be taken as a useful tool in dynamo simulations. We emphasize that the sensitivity to the use of hyperdiffusion reported in the present paper is peculiar to *large-scale* dynamos and does not apply to small-scale dynamos.

The magnetic field evolution is governed by the induction equation,

$$\frac{\partial\boldsymbol{B}}{\partial t} = \boldsymbol{\nabla}\times(\boldsymbol{u}\times\boldsymbol{B}) + (-1)^{n-1}\eta_n\nabla^{2n}\boldsymbol{B}\,, \qquad (1)$$

with $\boldsymbol{\nabla}\cdot\boldsymbol{B} = 0$, $\eta_n = \text{const}$, and $n = 1$ for ordinary magnetic diffusivity. This equation has to be integrated together with the momentum and continuity equations which are, for an isothermal compressible gas with constant speed of sound, c_s,

$$\frac{D\boldsymbol{u}}{Dt} = -c_s^2 \boldsymbol{\nabla} \ln\rho + \frac{\boldsymbol{J}\times\boldsymbol{B}}{\rho} + \boldsymbol{F}_{\rm visc} + \boldsymbol{f}, \quad (2)$$

$$\frac{D\ln\rho}{Dt} = -\boldsymbol{\nabla}\cdot\boldsymbol{u}, \quad (3)$$

where $D/Dt = \partial/\partial t + \boldsymbol{u}\cdot\boldsymbol{\nabla}$ is the advective derivative, $\boldsymbol{F}_{\rm visc} = \frac{\mu}{\rho}(\nabla^2\boldsymbol{u} + \frac{1}{3}\boldsymbol{\nabla}\boldsymbol{\nabla}\cdot\boldsymbol{u})$ is the viscous force, $\mu =$ const is the dynamical viscosity, c_s is the isothermal sound speed, $\boldsymbol{J} = \boldsymbol{\nabla}\times\boldsymbol{B}/\mu_0$ is the current density, and μ_0 is the vacuum permeability. As in B2001, the forcing function $\boldsymbol{f}(\boldsymbol{x},t)$ is a randomly chosen polarized wave taken from a band of wave numbers around the forcing wave number k_f. The direction and phase of $\boldsymbol{f}$ change randomly at each time step. We solve the equations in a periodic domain of size L^3, where $L = 2\pi$. We adopt nondimensional units by measuring density in units of the average value, $\rho_0 = \langle\rho\rangle$, length in units of $1/k_1$, where $k_1 = 2\pi/L = 1$ is the smallest wave number, velocity in units of c_s, magnetic field in units of $c_s\sqrt{\rho_0\mu_0}$, and time in units of $(c_s k_1)^{-1}$.

For numerical solutions, the smallest possible value of η_n is given by the condition that the mesh magnetic Reynolds number, based on the smallest scales resolved,

$$R_{\rm m}^{(\rm mesh)} = u_{\rm rms}/(\eta_n k_{\rm Ny}^{2n-1}), \quad (4)$$

is of order unity. Here $k_{\rm Ny} = \pi N/L$ is the Nyquist wave number of a mesh with N points.

As a reference model, we consider a calculation with ordinary magnetic diffusivity, $\eta_1 = 10^{-4}$, and a forcing wave number $k_f = 27$ (Run A). We adopt a dynamical viscosity of $\mu = 10^{-2}$, so the magnetic Prandtl number is 100. In Fig. 1 we show spectra at different times. Consistent with earlier results (B2001), magnetic energy grows owing to dynamo action with spectral peaks at the forcing scale, $k = k_f$, and at some intermediate scale, $k \approx 9$. By $t \approx 480$ (seventh curve from the bottom of Fig. 1) the intermediate scale field has reached equipartition with the kinetic energy; the field continues to grow, however, and now evolves towards larger scales under a k^{-1} envelope.

Qualitatively similar behavior is found for the hyperdiffusive Run B, with $\eta_2 = 3\times10^{-8}$; see Fig. 2. This case, which has similar diffusion at the Nyquist wave number to Run A, also exhibits a secondary peak at some intermediate wave number. Following B2001, cf. Eqs. (36)–(39) therein, we identify this with the wave number where growth rate of a corresponding α^2 dynamo model is maximum. In the initial kinematic stage, the position of the secondary peak is approximately constant in time ($k_{\rm max} \approx 9$ for Run A and $k_{\rm max} \approx 14$ for Run B). When the magnetic energy reaches equipartition with the kinetic energy, $E_{\rm kin}$, the secondary peak begins to travel toward smaller k. A reasonable fit to this migration is given by

$$k_{\rm max}^{-1} = \alpha_{\rm trav}(t - t_{\rm sat}), \quad (5)$$

where the parameter $\alpha_{\rm trav}$ characterizes the speed at which the intermediate peak travels. The values obtained from fits to these runs are listed in Table I, together with some other parameters defined below. Note that for Run C, with a lower hyperdiffusivity $\eta_2 = 10^{-8}$, the speed of the peak has decreased even further. This suggests that *even at intermediate scales* (i.e., k less than the initial value of $k_{\rm max}$), the dynamo process is resistively limited.

Since it is difficult to evolve a simulation at this resolution over a full large-scale diffusion time, $\sim(\eta_n k_1^{2n})^{-1}$, we now compare with a low resolution run with only 30^3 mesh points, $\eta_n = 10^{-4}$ (Run D). The parameters of this run are chosen so that the factor k_f^{2n-1}, which appears in the theory below, is consistent with Run A. The large-scale magnetic field shows a very prolonged saturation phase after the saturation of the small-scale field (and the

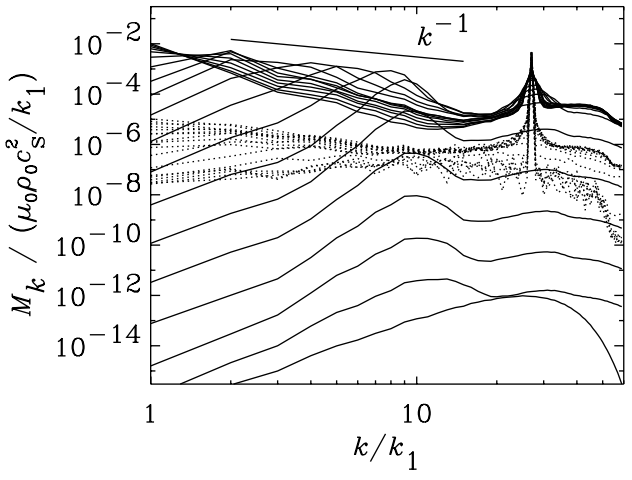

FIG. 1. Evolution of magnetic energy spectra in Run A (with ordinary magnetic diffusion) in equidistant time intervals at $t = 0$ (lowest curve), $t = 80$ (next one higher up), until $t = 1200$ (peaking at the very top left). The dotted lines give the kinetic energy.

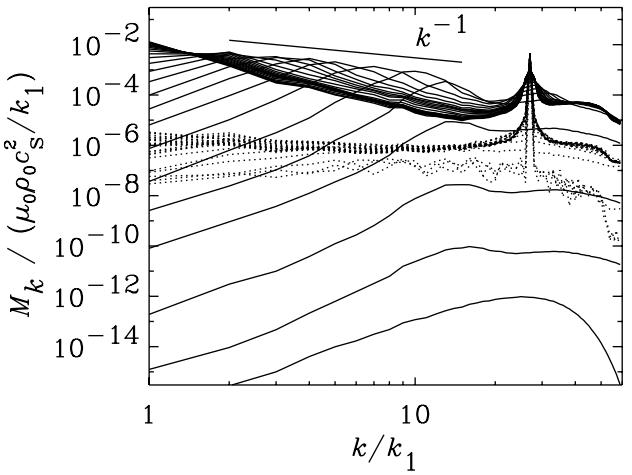

FIG. 2. Evolution of magnetic energy spectra in the hyperdiffusive Run B in equidistant time intervals at $t = 0$ (lowest curve), $t = 40$ (next one higher up), until $t = 2080$ (peaking at the very top left). The dotted lines give the kinetic energy.

TABLE I. Summary of the runs discussed in this paper. Note that $\alpha_{\rm trav}$ decreases with decreasing values of η_n. λ is the kinematic growth rate of the magnetic energy, H and M are, respectively, magnetic helicity and energy during the kinematic stage, and the parameter $\ell_{\rm skin}$ (defined below) gives an approximate upper bound for $\ell_{\rm H} \equiv |H|/(2\mu_0 M)$.

Run	N	n	η_n	λ	$k_{\rm f}$	$\alpha_{\rm trav}$	$\ell_{\rm H}$	$\ell_{\rm skin}$
A	120^3	1	10^{-4}	0.047	27	1.1×10^{-3}	0.035	0.065
B	120^3	2	3×10^{-8}	0.070	27	7.3×10^{-4}	0.018	0.025
C	120^3	2	10^{-8}	0.082	27	3.6×10^{-4}	0.005	0.013
D	30^3	2	10^{-4}	0.078	3	$\cdots$	0.08	0.15

equipartition of magnetic and kinetic energy), finally equilibrating only after approximately one large-scale diffusion time; see Fig. 3.

As in B2001, we can interpret the slow saturation behavior in terms of the magnetic helicity equation. We begin with the uncurled induction equation,

$$\frac{\partial \boldsymbol{A}}{\partial t} = \boldsymbol{u} \times \boldsymbol{B} + (-1)^{n-1}\eta_n \nabla^{2n}\boldsymbol{A} - \boldsymbol{\nabla}\phi\,, \qquad (6)$$

where $\boldsymbol{A}$ is the magnetic vector potential, with $\boldsymbol{B} = \boldsymbol{\nabla} \times \boldsymbol{A}$, and ϕ is the electrostatic potential which can be chosen arbitrarily without affecting $\boldsymbol{B}$. For a periodic domain of volume V, the magnetic helicity,

$$H = \int_V \boldsymbol{A} \cdot \boldsymbol{B}\, dV \equiv \langle \boldsymbol{A} \cdot \boldsymbol{B} \rangle V\,, \qquad (7)$$

where angular brackets denote volume averages, is independent of the choice of ϕ. (For the simulations we take $\phi = 0$.) Dotting Eq. (1) with $\boldsymbol{A}$, and Eq. (6) with $\boldsymbol{B}$, adding the two and averaging, yields

$$\frac{d}{dt}\langle \boldsymbol{A} \cdot \boldsymbol{B} \rangle = (-1)^n 2\eta_n \langle (\nabla^{2n}\boldsymbol{A}) \cdot \boldsymbol{B} \rangle\,. \qquad (8)$$

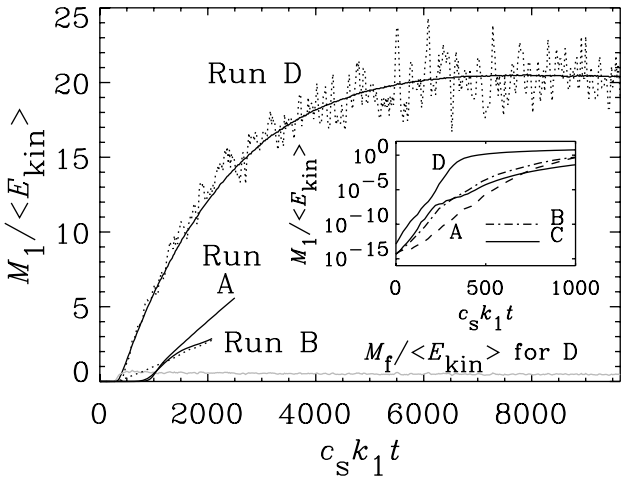

FIG. 3. Evolution of large-scale magnetic energy, normalized by the kinetic energy, for Runs A, B, and D. The dotted lines give the result expected from Eq. (15), as is explained below; these lines show strong fluctuations because we have used here the actual value of $M_{\rm f}$. For Run D, $M_{\rm f}$ is also shown (grey line at the very bottom). The inset shows the early kinematic evolution for Runs A–D in a semilogarithmic representation.

Surface terms are absent because of periodic boundaries. For this reason, and because $\boldsymbol{\nabla} \cdot \boldsymbol{B} = 0$, the right hand side of Eq. (8) becomes $-2\eta_1\langle \boldsymbol{J} \cdot \boldsymbol{B} \rangle$ when $n = 1$.

We now proceed analogously to B2001. First, in the steady state, $\langle \boldsymbol{A} \cdot \boldsymbol{B} \rangle$ must be constant and so $\langle (\nabla^{2n}\boldsymbol{A}) \cdot \boldsymbol{B} \rangle$ must vanish. This happens in such a way that there are contributions from the forcing scale and the large scale such that the two terms have opposite sign and cancel. We calculate the large-scale field, $\overline{\boldsymbol{B}} = \boldsymbol{\nabla} \times \overline{\boldsymbol{A}}$, by Fourier filtering around $k = 1$ (using integer bins), and the small-scale field, $\boldsymbol{b} = \boldsymbol{\nabla} \times \boldsymbol{a}$, as $\boldsymbol{b} = \boldsymbol{B} - \overline{\boldsymbol{B}}$. The characteristic wave numbers of these scales are $k_{\rm f}$ (for forcing or fluctuating scale) and k_1 (for smallest wave number). Making use of the fact that the magnetic field is nearly fully helical at small and large scales, we have

$$(-1)^n \langle (\nabla^{2n}\boldsymbol{a}) \cdot \boldsymbol{b} \rangle \approx \pm k_{\rm f}^{2n-1} \langle \boldsymbol{b}^2 \rangle\,, \qquad (9)$$

$$(-1)^n \langle (\nabla^{2n}\overline{\boldsymbol{A}}) \cdot \overline{\boldsymbol{B}} \rangle \approx \mp k_1^{2n-1} \langle \overline{\boldsymbol{B}}^2 \rangle\,, \qquad (10)$$

where the upper and lower signs are for positive and negative signs of the kinetic helicity of the forcing, respectively. Thus, the ratio of large- to small-scale magnetic energies, i.e., the degree of superequipartition, is

$$\frac{M_1}{M_{\rm f}} \equiv \frac{\langle \overline{\boldsymbol{B}}^2 \rangle}{\langle \boldsymbol{b}^2 \rangle} = \left(\frac{k_{\rm f}}{k_1}\right)^{2n-1} > 1\,. \qquad (11)$$

For $k_{\rm f} = 3$, normal diffusion ($n = 1$) gives superequipartition by a factor of 3; see B2001. For Run D ($n = 2$) we should have superequipartition by a factor of 27. The numerical result (Fig. 3, where $M_{\rm f}/\langle E_{\rm kin} \rangle \approx 0.5$) gives $M_1/M_{\rm f} \approx 44$. As we explain below, this has to do with the fact that the estimates in (9) and (10) are not quite accurate. Nevertheless, the effect of hyperdiffusivity on the level of superequipartition is clear.

Analogously to B2001 we can also calculate the asymptotic saturation behavior by using Eqs. (9) and (10) and assuming equipartition at small scales, $\langle \boldsymbol{b}^2 \rangle \approx \langle \rho \boldsymbol{u}^2 \rangle$, which is expected to hold after the time $t_{\rm s}$ when the small-scale field has saturated. (The fact that these solutions satisfy $M_{\rm f}/\langle E_{\rm kin} \rangle \approx 0.5$, rather than strict equipartition, does not affect the following.) This gives

$$k_1^{-1}\frac{d}{dt}\langle \overline{\boldsymbol{B}}^2 \rangle = -2\eta_n k_1^{2n-1} \langle \overline{\boldsymbol{B}}^2 \rangle + 2\eta_n k_{\rm f}^{2n-1} \langle \boldsymbol{b}^2 \rangle\,, \qquad (12)$$

which has the solution

$$\langle \overline{\boldsymbol{B}}^2 \rangle = \langle \boldsymbol{b}^2 \rangle \left(\frac{k_\mathrm{f}}{k_1} \right)^{2n-1} [1 - e^{-2\eta_n k_1^{2n}(t-t_\mathrm{s})}]. \quad (13)$$

In the early saturation phase, we have

$$\langle \overline{\boldsymbol{B}}^2 \rangle / \langle \boldsymbol{b}^2 \rangle \approx 2\eta_n k_1 k_\mathrm{f}^{2n-1}(t - t_\mathrm{s}). \quad (14)$$

Thus, Run A ($\eta_1 = 10^{-4}$ and $k_\mathrm{f} = 27$) and Run D ($\eta_2 = 10^{-4}$ and $k_\mathrm{f} = 3$) should exhibit the same saturation behavior; this can be approximately verified from the early saturation behavior visible in Fig. 3.

The magnetic field in Run D actually saturates somewhat faster than suggested by Eq. (13). Again, this is explained by the observation that the estimates for the effective values of the wave numbers in (9) and (10) are not accurate. Good agreement can be achieved if, instead, we use Eqs. (9) and (10) to calculate *effective* wave numbers, $k_1 \rightarrow k_{1,\mathrm{eff}}$ and $k_\mathrm{f} \rightarrow k_{\mathrm{f,eff}}$, for the large- and small-scale fields, respectively, and if we use the actual values for the small-scale magnetic energy, M_f (which shows a long-term trend, but is also fluctuating). For Run D we find $k_{1,\mathrm{eff}} = 1.3$ and $k_{\mathrm{f,eff}} = 4.6$. Such an enhancement results from hyperdiffusivity which increases the relative contributions from higher harmonics. The modified version of Eq. (13) is then

$$M_1 = M_\mathrm{f} \left(\frac{k_{\mathrm{f,eff}}}{k_{1,\mathrm{eff}}} \right)^{2n-1} [1 - e^{-2\eta_n k_1 k_{1,\mathrm{eff}}^{2n-1}(t-t_\mathrm{s})}]. \quad (15)$$

The evolution predicted by Eq. (15) is shown as dotted lines in Fig. 3. Note that the time taken for saturation is dependent upon the large-scale hyperdiffusion time $(\eta_n k_{1,\mathrm{eff}}^{2n})^{-1}$, but that since the large-scale field is of approximately unit wave number, $k_{1,\mathrm{eff}} \approx 1$, the hyperdiffusivity has very little effect, decreasing this time only slightly (cf. the true large-scale diffusion time for this value of η). In this respect, hyperdiffusivity is behaving exactly as we would wish, allowing us to attain low η at lesser computational expense, and with little effect on the physical behavior.

We note that during the *kinematic* phase the dynamo is still growing on a fast dynamical time scale. At this stage, the net magnetic helicity remains close to zero, as it must for the high magnetic Reynolds numbers under consideration. Berger's inequality [13] gives an upper limit for the growth of magnetic helicity, derived by bounding the right hand side of Eq. (8) via the square root of Joule dissipation and magnetic energy. In the presence of hyperdiffusivity this inequality is

$$\ell_\mathrm{H} \equiv |H|/(2\mu_0 M) \leq a\ell_\mathrm{skin}, \quad (16)$$

where $\ell_\mathrm{skin} = (2\eta_n k_\mathrm{f}^{2n-2}/\lambda)^{1/2}$ is a modified skin depth, λ is the kinematic growth rate of the magnetic energy, and a is a coefficient of order unity. From Table I we see that this constraint is indeed well satisfied during the kinematic growth phase.

The present results have demonstrated that hyperdiffusivity can have profound effects on dynamos with helicity. The modifying effects are well understood, which makes the use of hyperdiffusivity an efficient tool for numerical studies. This has allowed us here to show that helical dynamos saturate resistively both on large and intermediate scales, but not on small scales.

Use of the PPARC supported supercomputers in St Andrews and Leicester (UKAFF) is acknowledged.

[1] C. Basdevant *et al.,* J. Atmos. Sci. **38**, 2305 (1981); J. C. McWilliams, J. Fluid Mech. **146**, 21 (1984); T. Passot and A. Pouquet, J. Comput. Phys. **75**, 300 (1988).
[2] G. Falkovich, Phys. Fluid **6**, 1411 (1994); N. Schorghofer, L. Kadanoff, and D. Lohse, Physica (Amsterdam) **88A**, 40 (1995); D. Lohse and A. Müller-Groeling, Phys. Rev. Lett. **74**, 1747 (1995).
[3] D. H. Porter, A. Pouquet, and P. R. Woodward, Phys. Rev. Lett. **68**, 3156 (1992); D. H. Porter, P. R. Woodward, and A. Pouquet, Phys. Fluid **10**, 237 (1998).
[4] D. Biskamp and W.-C. Müller, Phys. Plasmas **7**, 4889 (2000).
[5] D. Biskamp, E. Schwarz, and A. Celani, Phys. Rev. Lett. **81**, 4855 (1998).
[6] D. Biskamp and E. Schwarz, Phys. Plasmas **8**, 3282 (2001).
[7] M. Meneguzzi, U. Frisch, and A. Pouquet, Phys. Rev. Lett. **47**, 1060 (1981); S. Kida, S. Yanase, and J. Mizushima, Phys. Fluid A **3**, 457 (1991); D. Biskamp and W.-C. Müller, Phys. Rev. Lett. **83**, 2195 (1999); J. Cho and E. Vishniac, Astrophys. J. **538**, 217 (2000); H. Chou, Astrophys. J. **556**, 1038 (2001); J. Maron and P. Goldreich, Astrophys. J. **554**, 1175 (2001).
[8] K.-K. Zhang and C. A. Jones, Geophys. Res. Lett. **24**, 103 (1997); K.-K. Zhang, C. A. Jones, and G. R. Sarson, Stud. Geophys. Geod. **42**, 247 (1998); G. R. Sarson, C. A. Jones, and A. W. Longbottom, Geophys. Astrophys. Fluid Dyn. **88**, 225 (1998).
[9] G. A. Glatzmaier and P. H. Roberts, Nature (London) **377**, 203 (1995); G. A. Glatzmaier and P. H. Roberts, Physica (Amsterdam) **97D**, 81 (1996); W. Kuang and J. Bloxham, Nature (London) **389**, 371 (1997).
[10] E. Grote, F. H. Busse, and A. Tilgner, Geophys. Res. Lett. **27**, 2001 (2000).
[11] S. I. Vainshtein and F. Cattaneo, Astrophys. J. **393**, 165 (1992); A. Bhattacharjee and Y. Yuan, Astrophys. J. **449**, 739 (1995); E. G. Blackman and G. B. Field, Astrophys. J. **534**, 984 (2000).
[12] A. Brandenburg, Astrophys. J. **550**, 824 (2001).
[13] M. Berger, Astrophys. Fluid Dyn. **30**, 79 (1984).